An image-based effective-medium modeling of near-surface anomalies

Oz Yilmaz, GeoTomo LLC

Near-surface modeling for statics corrections is an integral part of a land seismic data processing workflow. The methods for near-surface modeling can be categorized into five groups: (1) uphole surveys, (2) shallow seismic surveys, (3) traveltime inversion, (4) waveform inversion, and (5) joint inversion of seismic and nonseismic data. The first two are past methods, the third, usually referred to as traveltime tomography, is at present the most widely accepted method, and the last two methods are future methods with several practical aspects yet to be resolved.

I present an image-based workflow for modeling near-surface anomalies, which

1) does not require first-break picking as for traveltime tomography,
2) does not require source wavelet estimation as for waveform inversion,
3) does not fail velocity inversions as in traveltime tomography,
4) does not suffer from velocity-depth ambiguity,
5) does not require data (traveltime or wave-field) modeling as for any inversion method, and
6) does not exhaust computational resources as in waveform and joint inversions.

The method (termed *i*-stats) is based on prestack depth migration of shot records from a floating datum that closely resembles surface topography using a range of near-surface velocities. The resulting depth images form an image volume which can then be interpreted to pick the reflector associated with the base of the near surface and to pick the velocities for the near surface from the corresponding horizon-consistent semblance spectrum. The resulting 'effective-medium' model for the near surface comprises laterally varying velocities only, but yields essentially the same statics that one calculates from a more complicated model for the near surface that may be estimated from tomography or inversion methods. The effective-medium model of the near surface conforms to the vertical raypath assumption that underlies statics corrections. I demonstrate the *i*-stats method to correct for the deleterious effect of near-surface anomalies associated with sand dunes, shallow anhydrites, and glacial tills on subsurface reflections.

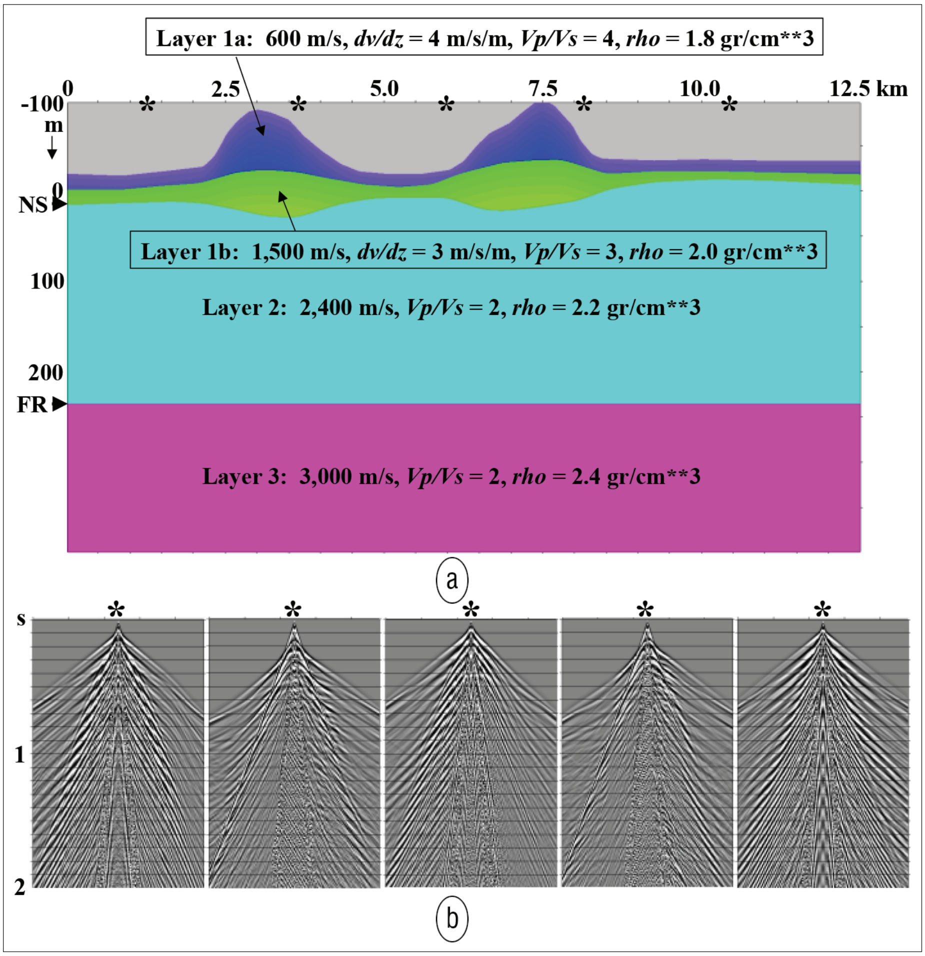

Figure 1. *(a) The velocity-depth model used for elastic wave-field modeling of shot records as in (b). The model consists of a near surface with two layers (1a,b) with vertical velocity gradients, and a subsurface with two layers (2 and 3) with a flat interface (FR). NS is the layer boundary between the near surface above and the subsurface below. Locations of the selected shot records are indicated by asterisks. Note the change in the dispersive characteristics of the Rayleigh-type surface waves from one shot gather to the next because of the change in thickness of the near-surface region and lateral velocity variations within the near surface.*

The *i*-stats workflow

I demonstrate the *i*-stats workflow by analyzing common-shot gathers generated by an elastic wave-field modeling algorithm (Larsen and Schultz, 1995) using a velocity-depth model that resembles sand dunes in the near surface (Figure 1). Sand dunes usually comprise a top layer of dry sand with low velocities (Layer 1a) and a base layer of wet sand with relatively higher velocities (Layer 1b). Both layers have vertical velocity gradients associated with compaction over the life time of the sand dune. An excellent study of sand dune velocities based on refraction surveys and laboratory measurements by Liner (2011) indicates that the sand curve—an empirical relationship between sand thickness and vertical one-way traveltime (Bridle et al., 2007) is useful for making initial statics corrections in areas where the sand base is uniformly flat. Nevertheless, in areas with irregular subdune topography, the sand curve cannot be applied routinely because of unknown local

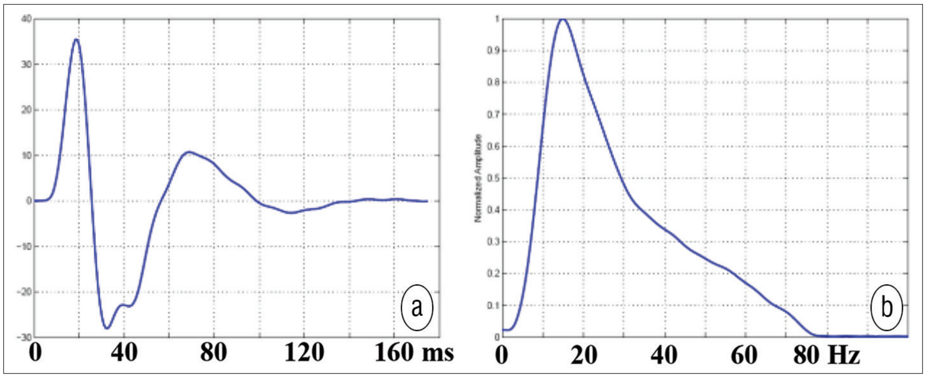

Figure 2. (a) Source wavelet used for elastic wave-field modeling of shot records as in Figure 1b and (b) its amplitude spectrum.

x-coordinate of the first shot	1200 m
Shot interval	25 m
Number of shots	380
Number of traces per shot	2401
Recording geometry	Split-spread
Minimum offset	0 m
Maximum offset	±1200 m
Receiver interval	1 m
Shot depth	3 m
Source wavelet bandwidth	Vertical-point force (Figure 2)
Sampling rate	1 ms
Recording length	2 s

Table 1. Sand-dunes line parameters for 2D elastic modeling of shot gathers.

variation in sand thickness (Liner, 2011). For such cases, an accurate near-surface model is required for statics corrections.

Listed in Table 1 are the recording parameters for the sand-dunes line. We used a source wavelet with dominant frequency of 15 Hz as shown in Figure 2.

Because of low shear-wave velocities in the near surface with a minimum value of 150 m/s (Figure 1), we used an extremely small grid size for modeling (dx X dz: 0.25 X 0.25 m). We then output shot gathers with 1-m receiver interval, and subsequently formed a linear receiver array of 25-m in length. The resulting shot gathers with 25-m shot interval and 25-m receiver interval were used in the *i*-stats workflow, as follows:

1) Apply elevation corrections to move the shots and receivers from surface topography to a floating datum that closely resembles the topographic variations with wavelengths greater than half the cable length using a velocity associated with the upper near surface.
2) Define the near-surface region as a half-space and perform prestack depth migration of all the shot gathers from the floating datum using a range of constant velocities associated with the near-surface velocity variations, and generate a set of image panels in depth (Figure 3a) accompanied with image gathers at intervals along the line traverse (Reshef, 1997; Yilmaz, 2001).
3) Scan the depth image panels and identify the shallowmost reflector that may be associated with the base of the near-surface region, and pick the depth horizon corresponding to that reflector (Figure 3a), while, if possible, paying attention to the flatness of the reflector event on the image gathers. You may be required to pick the depth horizon for the reflector under consideration from multiple image panels based on the highest image amplitude criterion.
4) Extract the horizon-consistent semblance spectrum along the picked depth horizon from within the depth image volume and pick the interval velocity strand along the line traverse (Figure 3b).
5) Combine the horizon strand from the depth image with the velocity strand from the semblance spectrum to build the effective-medium velocity-depth model for the near surface (Figure 3c).
6) Now calculate the shot-receiver statics to move the shots and receivers from the floating datum down to the intermediate datum represented by the depth horizon picked

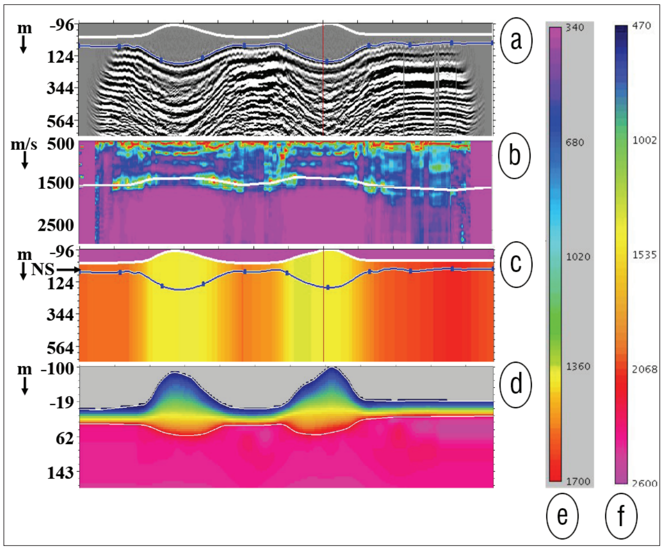

Figure 3. (a) Depth image panel generated by prestack depth migration of shot gathers from the floating datum represented by the white horizon (step 2 of the i-stats workflow) and the horizon picked along the shallow reflector that may be treated as the base of the near surface (step 3 of the i-stats workflow); (b) the horizon-consistent semblance spectrum extracted along the depth horizon in (a) from within the depth image volume and the image-based interval velocity strand picked from the semblance spectrum along the line traverse (step 4 of the i-stats workflow); (c) the effective-medium model of the near surface constructed by combining the horizon strand NS from the depth image shown in (a) with the velocity strand from the semblance spectrum shown in (b) (step 5 of the i-stats workflow); and (d) the near-surface velocity-depth model estimated by the application of nonlinear traveltime tomography to the first-arrival times picked form the shot gathers. The color spectra (e) and (f) for velocities in m/s correspond to the models shown in (c) and (d), respectively. The white horizons in (d) are the floating datum and the intermediate datum (which is not the same as the NS horizon in (c)) used in calculating the tomostatics shown in Figure 4b.

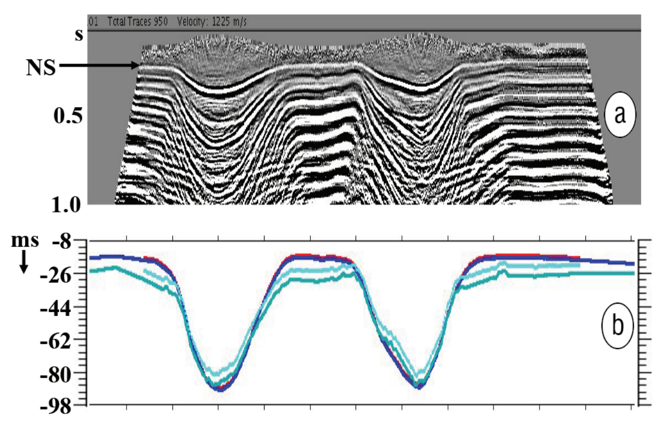

Figure 4. *(a) A constant-velocity stack panel with velocity that yields the highest stack amplitude for the event labeled as NS, which corresponds to the interface between the near surface and the subsurface (Figures 1a and 3c); (b) shot-receiver statics (red and blue, respectively) calculated from the i-stats effective-medium model shown in Figure 3c, shot-receiver statics (dark green) calculated from the tomographic model shown in Figure 3d, and shot-receiver statics (light green) calculated from the true model shown in Figure 1a.*

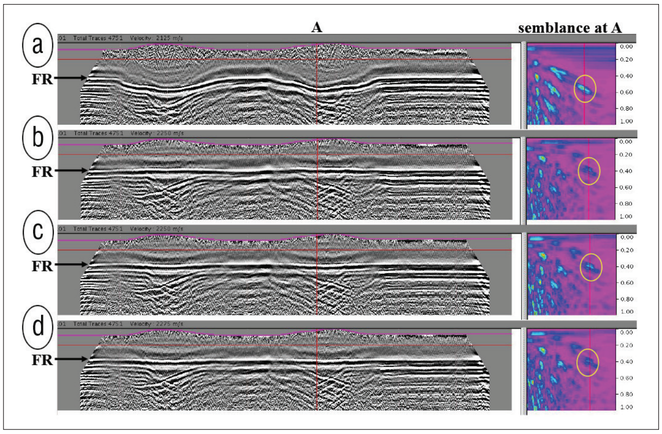

Figure 5. *Constant-velocity stack (CVS) panels with (a) elevation statics; (b) shot-receiver statics (Figure 4b) computed from the i-stats effective-medium model (Figure 3c); (c) shot-receiver statics (Figure 4b) computed from the tomographic model (Figure 3d); and (d) shot-receiver statics (Figure 4b) computed from the true model (Figure 1a). Each of the CVS panels was selected such that the corresponding velocity yields the highest stack amplitude for the event labeled as FR, which corresponds to the flat reflector shown in Figure 1a. The velocity range in the semblance spectra shown on the right is 500-3,000 m/s. The semblance peaks inside the white circles corrsepond to the event FR. All CVS panels are referenced to the same floating datum above the topography.*

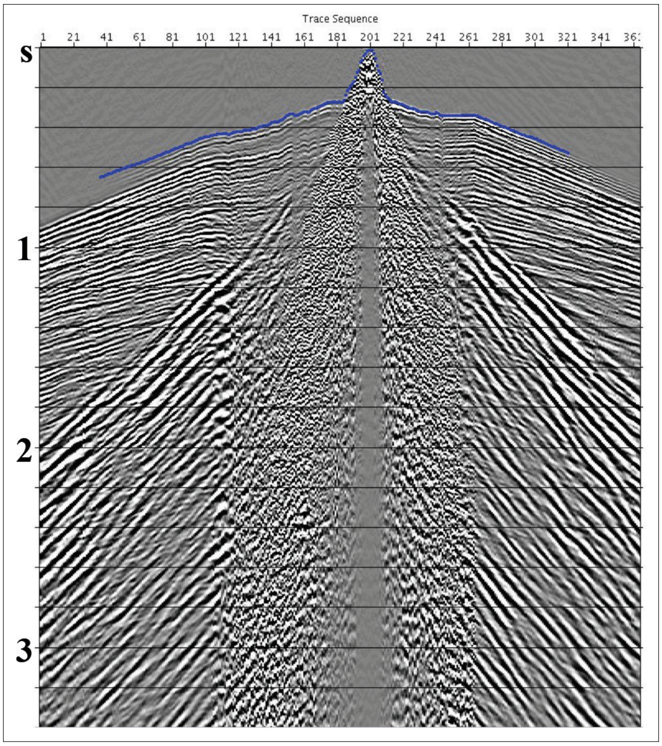

Figure 6. *A shot record along the line traverse associated with the data from case study 1. The receiver spread for this shot record is over a sand dune.*

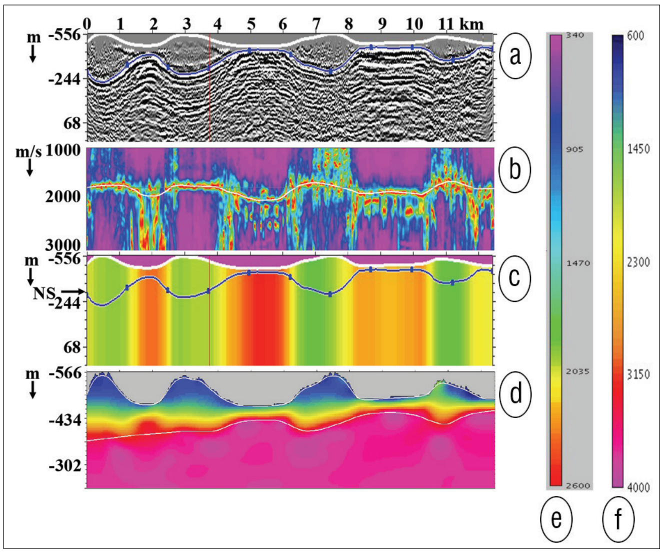

Figure 7. *Case study 1: (a) A depth image panel generated by prestack depth migration of shot gathers from the floating datum represented by the white horizon (step 2 of the i-stats workflow) and the horizon picked along the shallow reflector that may be treated as the base of the near surface (step 3 of the i-stats workflow); (b) the horizon-consistent semblance spectrum extracted along the depth horizon in (a) from within the depth image volume and the image-based interval velocity strand picked from the semblance spectrum along the line traverse (step 4 of the i-stats workflow); (c) the effective-medium model of the near surface constructed by combining the horizon strand NS from the depth image shown in (a) with the velocity strand from the semblance spectrum shown in (b) (step 5 of the i-stats workflow); and (d) the near-surface velocity-depth model estimated by the application of nonlinear traveltime tomography to the first-arrival times picked form the shot gathers. The color spectra (e) and (f) for velocities in m/s correspond to the models shown in (c) and (d), respectively. The white horizons in (d) are the floating datum and the intermediate datum (which is not the same as the NS horizon in (c)) used in calculating the tomostatics shown in Figure 8b.*

in step 3 using the effective-medium velocities (Figure 3c) and back up to the floating datum using an appropriate replacement velocity.

For comparison with the image-based effective-medium model (Figure 3c), Figure 3d shows the near-surface model estimated by nonlinear traveltime tomography (Zhang and Toksöz, 1998) applied to the first-arrival times picked from the field records. Irrespective of the method for near-surface

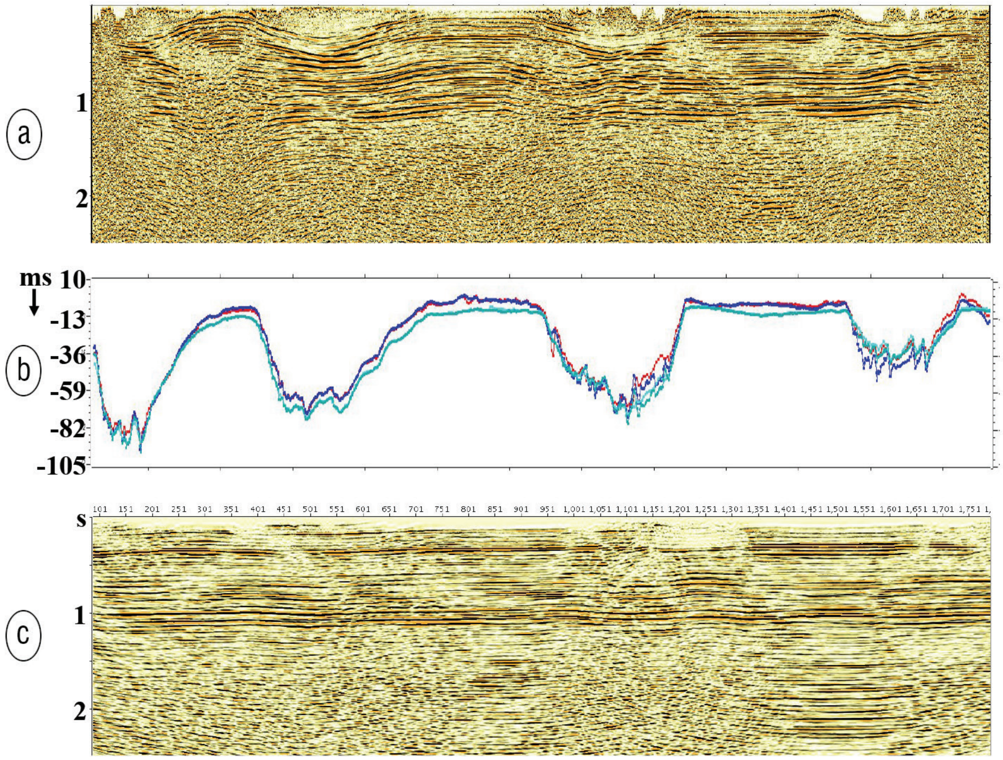

Figure 8. Case study 1: (a) CMP stack with elevation statics only; (b) shot-receiver statics (red and blue, respectively) calculated from the i-stats effective-medium model shown in Figure 7c combined with stack-power shot-receiver residual statics, and shot-receiver statics calculated from the tomographic model shown in Figure 7d (dark and light green, respectively); (c) image from prestack time migration (PSTM) of shot records with shot-receiver statics computed from the i-stats effective-medium model combined with stack-power shot-receiver residual statics as shown in (b).

modeling, the objective is to remove the deleterious effect of the near-surface anomaly on reflection traveltimes that is manifested by the stack shown in Figure 4a. Compare in Figure 4b the shot-receiver statics to those estimated by nonlinear traveltime tomography computed using the image-based effective-medium model. Note both methods yield almost equivalent long-wavelength results. Subsequent to the long-wavelength statics estimation, irrespective of the method used, short-wavelength residual statics estimation must follow (Yilmaz, 2001). Since the ultimate deliverables from the near-surface modeling are shot-receiver statics, not the near-surface model itself, which should be treated as an intermediate product, then, the image-based effective-medium modeling is just as valid as any other method for near-surface corrections. Moreover, the effective-medium model conforms more than any other method to the vertical-ray assumption underlying statics corrections.

A further comparison between the image-based effective-medium modeling and traveltime tomography is demonstrated by the constant-velocity stack (CVS) panels shown in Figure 5. The event labeled as FR corresponds to the flat reflector shown in Figure 1a. With the application of the shot-receiver statics calculated from both the *i*-stats workflow and the traveltime tomography, we have corrected for the effect of the near-surface anomalies associated with the sand dunes and restored the flat geometry of the subsurface reflector FR.

Case study 1: The sand dune problem

Shown in Figure 6 is a shot gather from a line traverse over sand dunes in North Africa. Receivers follow a nearly straight line over the dunes, while shots are placed around the dunes because vibrators could not be deployed over the top of the dunes composed of dry, loose sand. The distortions in the first-arrival times are caused by the irregular topography of the dunes and the complexity of the near-surface velocities, and the irregular shot-receiver geometry. The precursors associated with the klauder wavelet of the sweep signal on the correlated vibroseis record poses a challenge to automatic picking algorithms based on correlation and energy criteria applied to first-arrival waveforms. Therefore, I was compelled to manually pick the first breaks for all shot records. First-break picking and editing, especially for vibroseis data, is the most time consuming stage in near-surface modeling by traveltime tomography.

Figure 7 shows the stages in the *i*-stats workflow described above for near-surface modeling. For comparison, Figure 7d shows the near-surface model estimated by nonlinear traveltime tomography. This model accurately describes the anatomy of sand dunes: a low-velocity (around 500-600 m/s) cap on top of the dunes associated with dry sands, an interior with wet sands with velocity around 1,500 m/s, and a root with relatively higher velocity. The vertical velocity gradient within the sand dunes is a result of gradual accumulation of wind-swept sands within a topographic obstacle. Such a complex velocity field in the near surface gives rise to amplitude and traveltime distortions in moveout-corrected CMP gathers and thus in CMP stacked data (Figure 8a). Compare in Figure 8b the shot-receiver statics computed by nonlinear traveltime tomography and the shot-receiver statics computed by using the *i*-stats workflow. Again, the long-wavelength solution is almost equivalent. However, traveltime tomography consumed substantially more time to execute than the *i*-stats workflow because the former required accurate

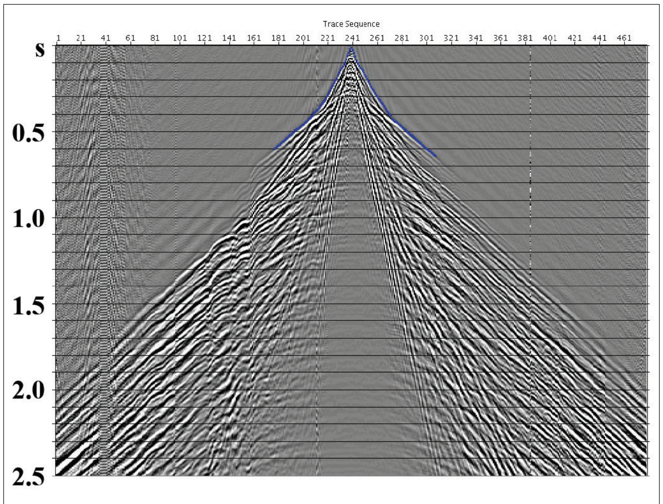

Figure 9. *A shot record along the line traverse associated with the data from case study 2.*

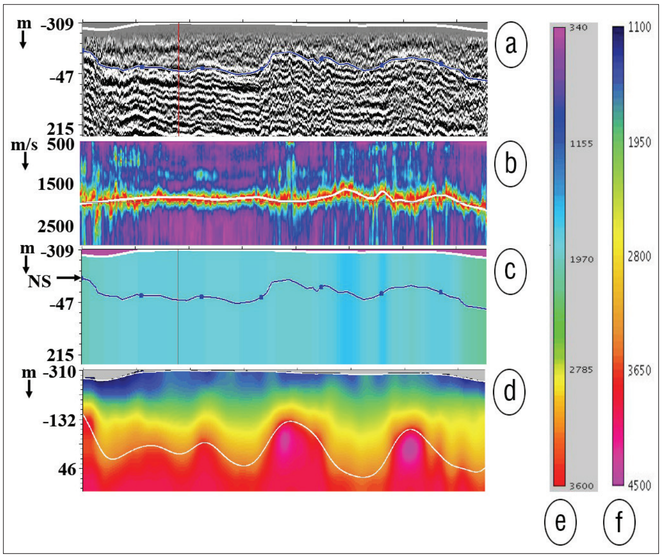

Figure 10. *Case study 2: (a) A depth image panel generated by prestack depth migration of shot gathers from the floating datum represented by the white horizon (step 2 of the i-stats workflow) and the horizon picked along the shallow reflector that may be treated as the base of the near surface (step 3 of the i-stats workflow); (b) the horizon-consistent semblance spectrum extracted along the depth horizon in (a) from within the depth image volume and the image-based interval velocity strand picked from the semblance spectrum along the line traverse (step 4 of the i-stats workflow); (c) the effective-medium model of the near surface constructed by combining the horizon strand NS from the depth image shown in (a) with the velocity strand from the semblance spectrum shown in (b) (step 5 of the i-stats workflow); and (d) the near-surface velocity-depth model estimated by the application of nonlinear traveltime tomography to the first-arrival times picked form the shot gathers. The color spectra (e) and (f) for velocities in m/s correspond to the models shown in (c) and (d), respectively. The white horizons in (d) are the floating datum and the intermediate datum (which is not the same as the NS horizon in (c)) used in calculating the tomostatics shown in Figure 11b.*

picking of the first breaks. Figure 8c shows the image from prestack time migration (PSTM) of shot records with statics corrections computed from the effective-medium near-surface model (Figure 7c). Compare with the stack section in Figure 8a and note that we have indeed removed the deleterious effect of the near-surface complexity associated with the sand dunes on the subsurface reflector geometry.

Case study 2: The buried statics problem

Shown in Figure 9 is a shot gather from a Middle East seismic line. The distortions in the first-arrival times are caused by irregular geometry of a shallow anhydrite layer and complexity of the near-surface velocities. Manual picking of the first breaks was again required for all shot records along the line traverse.

Figure 10 shows the stages in the *i*-stats workflow described above for near-surface modeling. For comparison, Figure 10d shows the near-surface model estimated by nonlinear traveltime tomography. This model exhibits the complexity of the near-surface anhydrite layer, which, if not corrected for, would give rise to amplitude and traveltime distortions in moveout-corrected CMP gathers and thus in CMP stacked data (Figure 11a). Compare in Figure 11b the shot-receiver statics computed by using the near-surface model estimated by nonlinear traveltime tomography and the shot-receiver statics computed by using the image-based effective-medium model estimated by the *i*-stats workflow. With respect to the long-wavelength solution for the shot-receiver statics, both methods yield almost equivalent results. Figure 11c shows the image from prestack time migration (PSTM) of shot records with statics corrections computed from the effective-medium near-surface model (Figure 10c) estimated by the *i*-stats method. Compare with the stack section in Figure 11a and note that we have indeed removed the deleterious effect of the near-surface complexity associated with the shallow anhydrite layer on the subsurface reflector geometry.

Case study 3: The glacial till problem

Shown in Figure 12 is a shot gather from a seismic line from Western Canada. The distortions in the first-arrival times are caused by the irregular geometry of the shallow glacial till layer. Figure 13 shows the stages in the *i*-stats workflow described above for near-surface modeling. For comparison, Figure 13d shows the near-surface model estimated by nonlinear traveltime tomography. This model exhibits the low-velocity glacial till layer, which gives rise to amplitude and traveltime distortions in CMP stacked data (Figure 14a). With respect to the long-wavelength solution for the shot-receiver statics, both traveltime tomography and the *i*-stats workflow methods yield almost equivalent results (Figure 14b). With statics corrections computed from the effective-medium near-surface model, the effect of the near-surface complexity associated with the glacial till on the subsurface reflector geometry has been removed in the image from prestack time migration (PSTM) of shot records (Figure 14c).

Conclusions

The *i*-stats method is an image-based effective-medium near-surface modeling method. It does not require first-break picking as for traveltime tomography, does not require

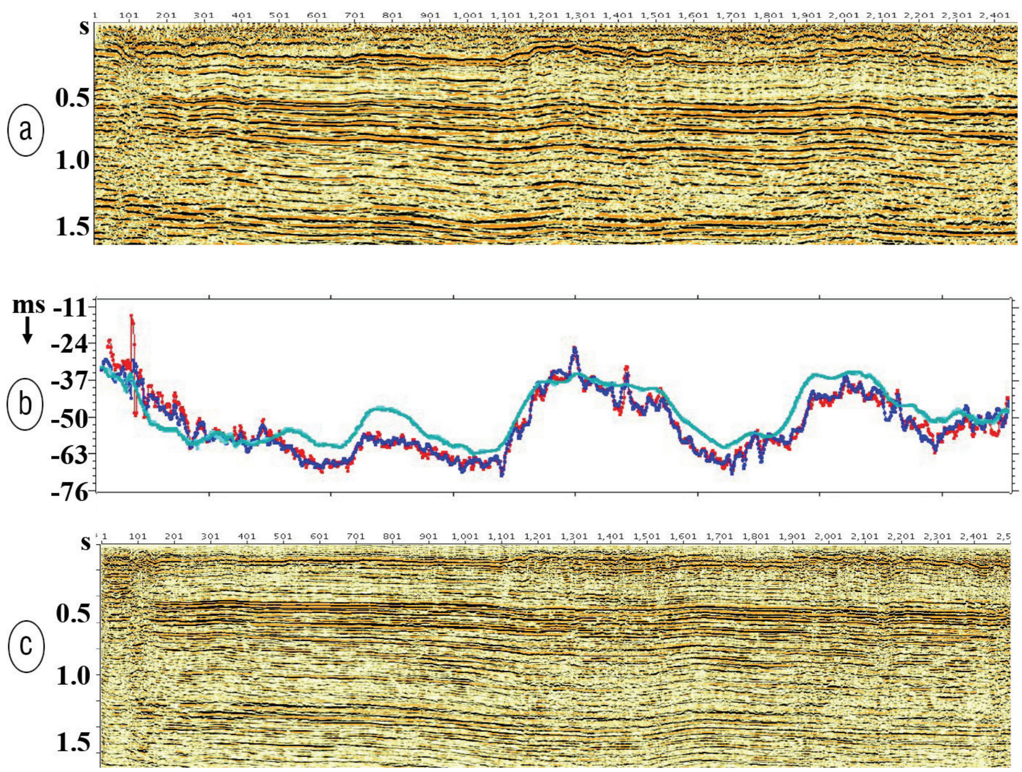

Figure 11. Case study 2: (a) CMP stack with elevation statics only; (b) shot-receiver statics (red and blue, respectively) calculated from the i-stats effective-medium model shown in Figure 10c combined with stack-power shot-receiver residual statics, and shot-receiver statics calculated from the tomographic model shown in Figure 10d (green); (c) image from prestack time migration (PSTM) of shot records with shot-receiver statics computed from the i-stats effective-medium model combined with stack-power shot-receiver residual statics as shown in (b).

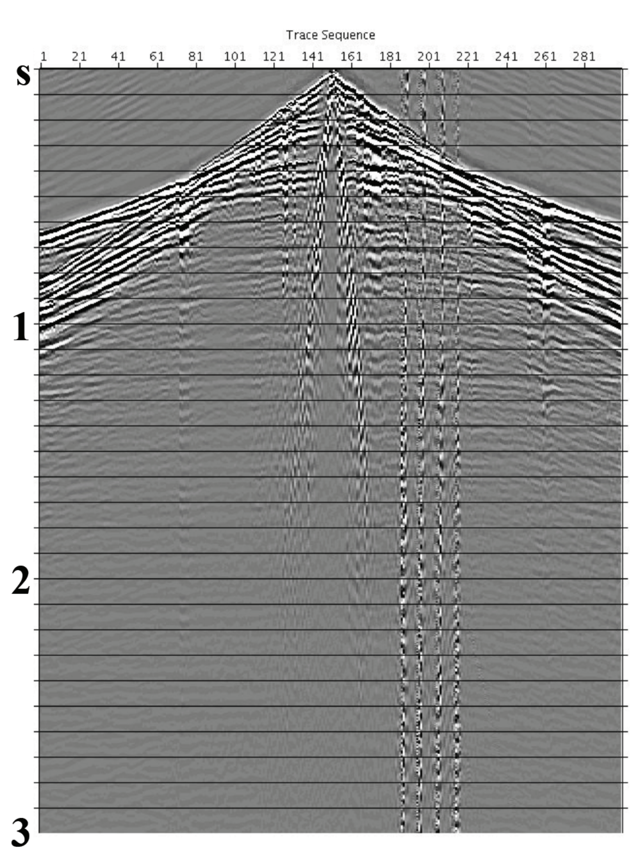

Figure 12. A shot record along the line traverse associated with the data from case study 3.

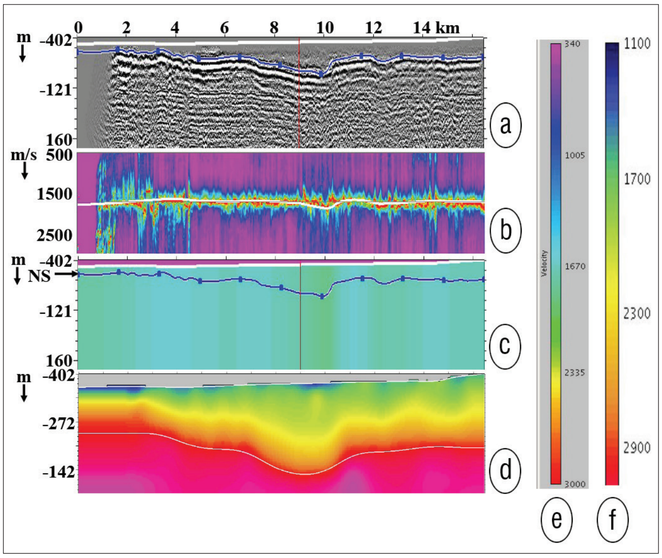

Figure 13. Case study 3: (a) Depth image panel generated by prestack depth migration of shot gathers from the floating datum represented by the white horizon (step 2 of the i-stats workflow) and the horizon picked along the shallow reflector that may be treated as the base of the near surface (step 3 of the i-stats workflow); (b) the horizon-consistent semblance spectrum extracted along the depth horizon in (a) from within the depth image volume and the image-based interval velocity strand picked from the semblance spectrum along the line traverse (step 4 of the i-stats workflow); (c) the effective-medium model of the near surface constructed by combining the horizon strand NS from the depth image shown in (a) with the velocity strand from the semblance spectrum shown in (b) (step 5 of the i-stats workflow); and (d) the near-surface velocity-depth model estimated by the application of nonlinear traveltime tomography to the first-arrival times picked form the shot gathers. The color spectra (e) and (f) correspond to the models shown in (c) and (d), respectively. The white horizons in (d) are the floating datum and the intermediate datum (which is not the same as the NS horizon in (c)) used in calculating the tomostatics shown in Figure 14b.

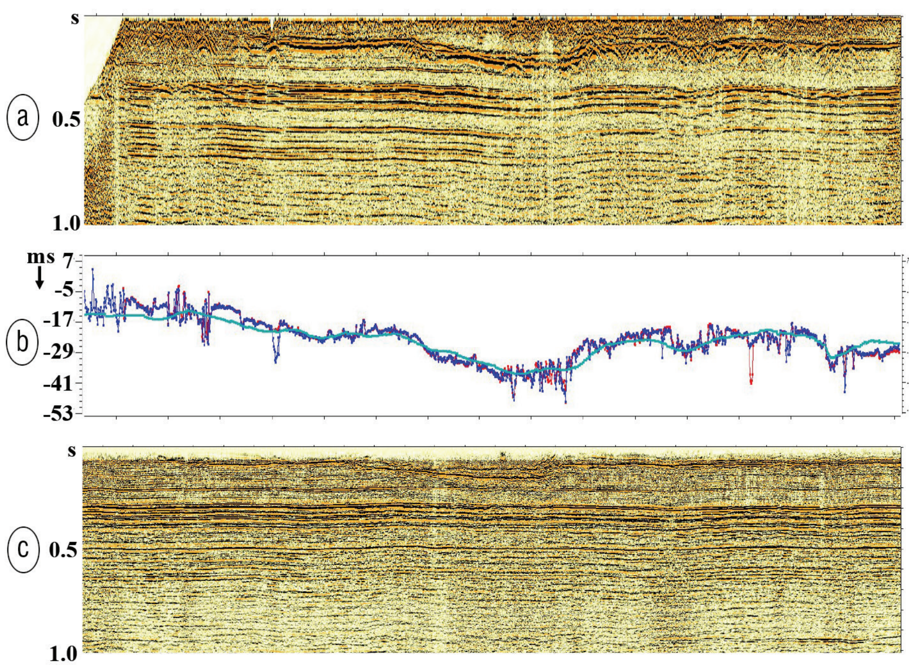

Figure 14. *Case study 3: (a) CMP stack with elevation statics only; (b) shot-receiver statics (red and blue, respectively) calculated from the i-stats effective-medium model shown in Figure 13c combined with stack-power shot-receiver residual statics, and shot-receiver statics calculated from the tomographic model shown in Figure 13d (green); (c) image from prestack time migration (PSTM) of shot records with shot-receiver statics computed from the i-stats effective-medium model combined with stack-power shot-receiver residual statics as shown in (b).*

source wavelet estimation as for waveform inversion, does not fail velocity inversions as in traveltime tomography, does not suffer from velocity-depth ambiguity, and does not exhaust computational resources as in waveform and joint inversions. I have demonstrated the *i*-stats workflow to resolve the near-surface anomalies associated with sand dunes, buried statics, and glacial till anomalies in the near surface. Although the examples given are for 2D seismic lines, the *i*-stats method also is readily applicable to 3D land seismic data.

The *i*-stats method was conceived as a result of two aspects of near-surface modeling and near-surface corrections:

1) Based on years of experience in the seismic industry, it is almost unreservedly evident for us all that, despite the theoretical favoritism for dynamic corrections, statics corrections are more than sufficiently accurate to remove the effect of near-surface anomalies on subsurface reflection geometries so long as an accurate model for the near surface is estimated. This statement is based on the axiom that, in contrast with the subsurface composed of relatively high-velocity, consolidated layers of rocks, the near surface is composed of low-velocity, unconsolidated, and often heterogeneous, weathered material with vertical and lateral velocity variations that are smaller in wavelength compared to the subsurface velocity variations.
2) The accuracy of the near-surface model estimated by traveltime tomography depends on the picking accuracy of the first-arrival times. Waveform inversion requires valid estimation of source wavelet and computationally intensive elastic wave-field modeling using an extremely small grid size to accommodate low velocities in the near surface. Joint inversion (of seismic and nonseismic data) is mathematically ill-posed; as such, the estimated near-surface model consistent with the seismic data is not necessarily consistent with the nonseismic data.

In contrast with tedious first-break picking in traveltime tomography, the *i*-stats method is based on event and semblance picking—interpretively appealing to the practicing geophysicist. In contrast with the yet-to-be-resolved practical aspects of waveform inversion and joint inversion methods, the intuitively appealing image-based *i*-stats method is extremely robust and efficient for modeling of near-surface anomalies. TLE

References

Bridle, R., R. Ley II, and A. Al-Mustafa, 2007, Near-surface models in Saudi Arabia: Geophysical Prospecting, **55**, no. 6, 779–792, http://dx.doi.org/10.1111/j.1365-2478.2007.00639.x.

Larsen, S. and C. A. Schultz, 1995, ELAS3D: 2D/3D elastic finite-difference wave propagation code, Lawrence Livermore National Laboratory Technical Report No. UCRL-MA-121792, 19 pp.

Liner, C., 2008, The seismic sand curve revisited: Geophysics, **73**, no. 1, A7–A10, http://dx.doi.org/10.1190/1.2817485.

Reshef, M., 1997, The use of 3D prestack depth imaging to estimate layer velocities and reflector positions: Geophysics, **62**, no. 1, 206–210, http://dx.doi.org/10.1190/1.1444120.

Yilmaz, O., 2001, Seismic Data Analysis, SEG, Tulsa, OK.

Zhang, J. and M. N. Toksöz, 1998, Nonlinear refraction traveltime tomography: Geophysics, **63**, no. 5, 1726–1737, http://dx.doi.org/10.1190/1.1444468.

Acknowledgments: I sincerely thank the oil companies who wanted to remain anonymous for providing the field records for the three case studies. I also am grateful to Professor Argun Kocaoglu of Istanbul Technical University for setting up and running the jobs on a cluster using the elastic wave-field modeling program of Larsen and Schultz (1995) to create the shot gathers for the sand dunes line as in Figure 1b. I am also grateful to Shaun Larsen to grant permission to use the elastic wave-field modeling program.

Corresponding author: oz@anatoliangeo.com